



Contents lists available at ScienceDirect

Journal of the Mechanics and Physics of Solids

journal homepage: www.elsevier.com/locate/jmps

A new thermo-mechanical coupled DEM model with non-spherical grains for thermally induced damage of rocks

Zhiqiang Chen^a, Xu Jin^b, Moran Wang^{a,*}

^a Department of Engineering Mechanics and CNMM, Tsinghua University, Beijing 100084, China

^b National Energy Tight Oil & Gas Research Centre, Petroleum Geology Research & Laboratory Center, Research Institute of Petroleum Exploration & Development (RIPE) PetroChina, Beijing 100083, China

ARTICLE INFO

Article history:

Received 12 February 2018

Revised 26 March 2018

Accepted 28 March 2018

Available online 29 March 2018

Keywords:

Thermo-mechanical coupled process

Non-spherical grains

Discrete element method

Thermally induced damage

ABSTRACT

Thermally induced damage often occurs in rocks in geophysical systems. Discrete element method (DEM) is a useful tool to model this thermo-mechanical coupled process owing to its explicit representation of fracture initiation and propagation. However, the previous DEM models for this are mostly based on spherical discrete elements, which are not able to capture all consequences (e.g. high ratio of compressive to tensile strength) of real rocks (e.g. granite) composed of complex-geometry grains. In order to overcome this intrinsic limitation, we present a new model allowing to mimick thermally induced damage of brittle rock with non-spherical grains. After validations, the new model is used to study thermal gradient cracking with a special emphasis on the effects from rock heterogeneity. The obtained fracture initiation and propagation are consistent with experimental observations, which demonstrates the ability of current model to reproduce the thermally induced damage of rocks. Meanwhile, the results show that rock heterogeneity influences thermal gradient cracking significantly, and more micro cracks uniformly scattering around the borehole are induced in the heterogeneous sample, which is not good for applications such as nuclear waste disposal. The present model provides a promising approach at micro-scale to explore mechanisms of thermally induced damage of rocks in geological engineering.

© 2018 Elsevier Ltd. All rights reserved.

1. Introduction

Understanding of thermally induced damage of rocks is of significance for a wide range of geological engineering such as nuclear waste disposal (Heard, 1989; Kim et al., 2011) and geothermal exploration (AbuAisha et al., 2016; Pandey et al., 2017). In deep geologic storage of nuclear waste, the temperature of host rock near the nuclear waste will increase owing to the decay of radioactive substance (Kim et al., 2011), which results in the temperature gradient and therefore induces thermal stress in rock (Jansen et al., 1993). When thermal stress exceeds the local strength of rock cracking happens, which forms the potential pathway for nuclear leakage (Heard, 1989; Jansen et al., 1993). Thermally induced damage also occurs in geothermal exploration process, where cold water with high pressure is injected into the underground geothermal reservoir to generate artificial fractures for permeability enhancement (AbuAisha et al., 2016).

For a better understanding of this thermo-mechanical coupled process, a lot of efforts have been made to numerically reproduce the fracturing behavior of rocks under thermal stress and to attempt to provide suggestions for geological engi-

* Corresponding author.

E-mail address: mrwang@tsinghua.edu.cn (M. Wang).

neering (Jiao et al., 2015; Lee and Ghassemi, 2010; Li et al., 2016; Wanne and Young, 2008; Wei et al., 2015). Continuum-based methods including finite element method (FEM) are not well suitable to simulate this process in discrete systems (Neveu et al., 2016), because complex fracturing behavior in rocks, such as cracking nucleation, coalescence and propagation, is difficult to be captured with continuum framework. Conversely, discontinuum-based methods provide a promising way to explore what happens in rock under thermal stress (Wanne and Young, 2008; Zhao, 2016). Among them, discrete element method (DEM) is a popular one owing to its good performance in simulating dynamic behavior of granular materials (e.g. soil and rock) (Potyondy and Cundall, 2004; Scholtès et al., 2011). Contrary to the continuum-based methods (e.g. FEM), the fracture behavior in DEM is explicitly represented, which enables it to capture the crack initiation and propagation processes efficiently. In addition, the discontinuous and heterogeneous natures of rocks can be easily considered in the framework of DEM. Therefore, DEM constitutes a powerful tool to explore the mechanisms of rock fracturing at micro scale.

Recently, DEM has been combined with heat conduction solving methods to study thermo-mechanical coupled processes (Wanne and Young, 2008; Xia et al., 2014; Zhao, 2016), where the rock is regarded as a collection of spherical discrete elements. However, some intrinsic limitations exist in these models, because DEM using spherical elements cannot capture all the consequences of real rocks (e.g. granite) composed of non-spherical grains (Galindo-Torres et al., 2010; Neveu et al., 2016; Scholtès and Donzé, 2013). For example, the classical DEM using spherical elements greatly underestimates the ratio of compressive to tensile strength regardless of whatever predefined values of parameters used (Potyondy and Cundall, 2004; Scholtès and Donzé, 2013). It is because the spherical elements cannot efficiently capture the grain-interlocking effect in real rocks composed of non-spherical grains. As a result, these models can hardly match properly both tensile strength and compressive strength simultaneously within a reasonable range (Potyondy and Cundall, 2004). Although some efforts have been made to overcome this limitation, including using non-spherical elements (Kawamoto et al., 2016; Kawamoto et al., 2018; Neveu et al., 2016) or making modification based on spherical elements (Bierwisch et al., 2009; Scholtès and Donzé, 2013), none of them are coupled with heat conduction to study the thermo-mechanical coupled process.

Thus, the objective of this paper is to present a thermo-mechanical coupled DEM formulation capable of properly simulating rock fracturing behavior, where non-spherical elements are developed. This model is based on discrete spheropolyhedra element method (DSEM) developed in (Galindo-Torres et al., 2012), which can capture the characteristics of irregular grains in real rocks with high computation efficiency. In this work, the thermal analysis function is developed and incorporated into the framework of DSEM, where heat conduction is solved by the lattice Boltzmann method (LBM) and thermal strain is considered by changing the size of spheropolyhedra element proportionally with the temperature change. After description and validations of current thermo-mechanical coupled DEM model, rock cracking caused by temperature gradient (thermal gradient cracking) will be simulated with an emphasis on the rock heterogeneity effects on this process. It will be shown that the proposed approach can provide good agreements with experimental observations in the description of thermally induced damage process at micro scale in terms of the fracture initiation and propagation. In addition, current results may provide some basic suggestions for nuclear waste disposal.

In the following, Section 2 gives a comprehensive description of current thermo-mechanical coupled model. Section 3 presents the validation of the new model by comparing with analytical solutions. Thermal gradient cracking process is simulated in Section 4, and in the last part, the paper is concluded.

2. Numerical methods

In this section, the proposed thermo-mechanical coupled model is introduced. First, current discrete element method (DEM) for rock failure simulation is described with an emphasis on its thermal analysis function. Then a brief introduction of the lattice Boltzmann method (LBM) for solving heat conduction process is given.

2.1. Discrete element method

In order to capture the grain interlocking effect, cemented geomaterials (e.g. rock) should be represented by a collection of polyhedra-shaped particles, which interact with each other through collision and cohesive force. However, the contact detection and the interaction force calculation of polyhedra-shaped particles in DEM are time-consuming. Thus, to improve computation efficiency, polyhedra-shaped particles in current DEM are represented by spheropolyhedra ones, which was proposed in (Galindo-Torres et al., 2012) and has achieved great success in simulating the failure behavior of geomaterials (Behrafter et al., 2017; Chen and Wang, 2017; Chen et al., 2018). Spheropolyhedra have similar dimensions with polyhedra but with rounded corners, which is generated by eroding and then dilating the polyhedra with a sphere element (termed as erosion sphere) (see Fig. 1). The basic framework of spheropolyhedra based DEM has been incorporated into the open source library MechSys, and only a brief introduction is provided in the following part. More focus of this subsection is paid on the thermal analysis function including a detail description of temperature effect on spheropolyhedra elements and its algorithm implementation.

2.1.1. Basic DEM framework

Similar to the classical DEM, current algorithm involves two basic steps. First, interaction force (collision and cohesive force) is calculated according to the displacement-force law. Then Newton's second law is integrated to determine the particle position and velocity at next time step. The above two steps are repeated until the simulation is finished.

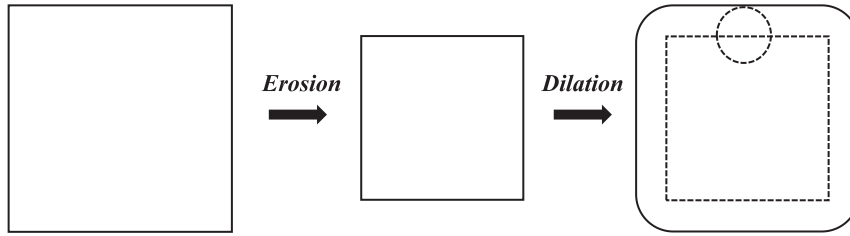


Fig. 1. Spheropolyhedra is generated by eroding and then dilating the polyhedra with a sphere element (termed as erosion sphere), whose radius is much smaller than the polyhedra size (Galindo-Torres et al., 2010).

The collision force arises when two particles collide with a small overlapping length Δl . It can only support compressive force \mathbf{F}_n^{cont} at normal direction and shear force \mathbf{F}_t^{cont} at tangential direction. They are given by the linear elastic model (Cundall and Strack, 1979)

$$\begin{cases} \mathbf{F}_n^{cont} = K_n \Delta l_n \mathbf{n} \\ \mathbf{F}_t^{cont} = K_t \Delta l_t \mathbf{t} \end{cases}, \quad (1)$$

where K_n and K_t are normal and tangential spring stiffness, Δl_n and Δl_t are the overlapping length in normal and tangential direction.

To model bonding, cohesive force \mathbf{F}_n^{cohe} and \mathbf{F}_t^{cohe} are assumed at the common face shared by two adjacent particles to oppose their relative motion at normal and tangential direction respectively. Cohesive force is linearly calculated according to the relative strain between two adjacent particles

$$\begin{cases} \mathbf{F}_n^{cohe} = M_n^{cohe} A \varepsilon_n \mathbf{n} \\ \mathbf{F}_t^{cohe} = M_t^{cohe} A \varepsilon_t \mathbf{t} \end{cases}, \quad (2)$$

where M_n^{cohe} and M_t^{cohe} are the normal and tangential elastic modulus of the assumed “bond” material, A is the shared face area, ε_n and ε_t are the strains of two adjacent particle faces in normal and tangential direction. A maximum acceptable strain threshold value ε_{th} is set for de-bonding judgment. When the following criterion is satisfied

$$\frac{|\varepsilon_n| + |\varepsilon_t|}{\varepsilon_{th}} > 1, \quad (3)$$

the bond is broken and a micro crack forms at the corresponding position. In addition, once the bond is broken, cohesive force vanishes and is no longer able to oppose the relative displacement between two adjacent particles.

2.1.2. Temperature effect

Thermal stresses are “stresses that result when a temperature change of material occurs in the presence of constraints” (Barron and Barron, 2011). Thus, thermal stresses are actually mechanical stress resulting from forces caused by a part attempting to expand or contract when it is constrained. The constraints may come from the external obstacle (external constraint) or from the material itself (internal constraint which means material expands or contracts by different amounts in various location). In current model, temperature change can produce thermal strains via particle thermal expansion. If this thermal expansion is constrained, thermal stress occurs. It is a common approach to consider the temperature effect in DEM and has achieved great success in simulating thermo-mechanical coupled process (Wanne and Young, 2008; Zhao, 2016).

In isothermal condition, particle size is fixed at a constant value during simulation, but in thermo-mechanical coupled DEM model, temperature change produces thermal strains via thermal expansion, so particle size varies with time. For spherical particles, this can be easily achieved by changing the radius of the particle. However, for non-spherical particles, how to change the particle size efficiently in the algorithm is a big challenge. Fortunately, in the framework of spheropolyhedra, this difficulty can be overcome by modifying the radius of erosion sphere with temperature change. By doing this, the change of non-spherical particle size can be efficiently achieved with little additional computational cost. The detail is presented in the following.

Here, two kinds of spheropolyhedra are taken as examples to illustrate current algorithm in dealing with non-spherical particle size change with temperature. For a square element with length l_T^0 at temperature T (see Fig. 2), thermal strain induced by the temperature change ΔT is considered by changing its length as

$$l_{T+\Delta T}^0 = l_T^0 + \alpha \Delta T l_T^0, \quad (4)$$

where α is thermal expansion coefficient. In sphero-square, this corresponding size change can be achieved by only changing the radius of erosion sphere as

$$r_{T+\Delta T} = r_T + l_T^0 / 2 \alpha \Delta T. \quad (5)$$

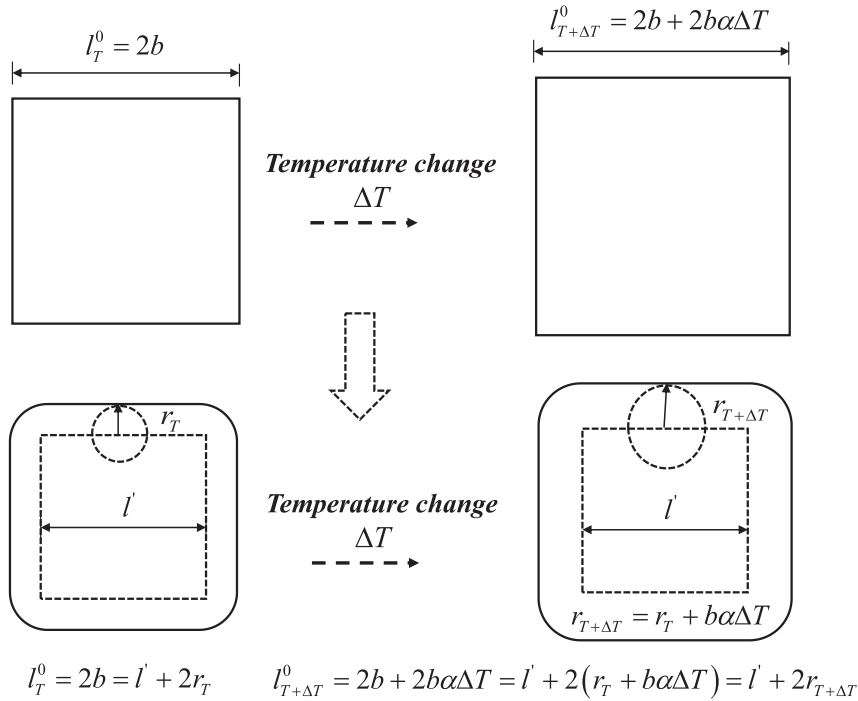


Fig. 2. Schematic to show particle size change achieved by modifying the radius of erosion sphere in sphero-square.

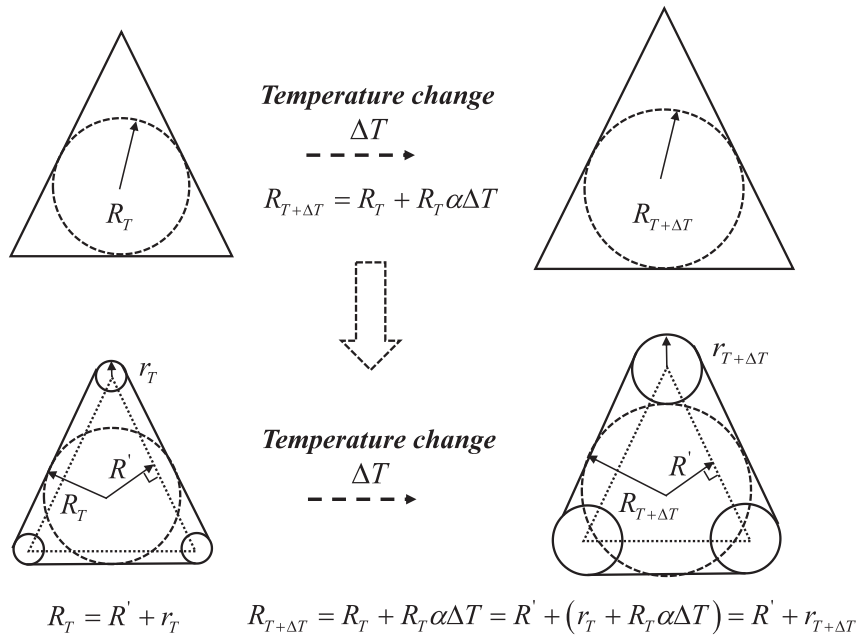


Fig. 3. Schematic to show particle size change achieved by changing the radius of erosion sphere in sphero-triangle.

For an arbitrary triangular element with radius of inscribed circle R at temperature T , given a temperature change ΔT , the triangular element will expand with similar shape to itself and the radius of its inscribed circle becomes

$$R_{T+\Delta T} = R_T + \alpha R_T \Delta T. \tag{6}$$

Similarly, triangular element size change with temperature can also be represented by changing the radius of erosion sphere as (see Fig. 3)

$$r_{T+\Delta T} = r_T + \alpha R_T \Delta T. \quad (7)$$

Thus, in the framework of sphero-polyhedra, particle thermal expansion induced by the temperature change can be generally achieved by changing the radius of erosion sphere

$$r_{T+\Delta T} = r_T + \alpha L_c \Delta T, \quad (8)$$

where α is thermal expansion coefficient, ΔT is temperature change, L_c is the characteristic length of sphero-polyhedra at reference temperature T , for square and triangle, which equals to half the length of the square (b in Fig. 2) and the radius of the inscribed circle (R_T in Fig. 3), respectively.

Besides the particle size, thermal strain also influences the cohesive normal force (\mathbf{F}_n^{cohe}) owing to the expansion or contraction of virtual bond beam (Wanne and Young, 2008), which is considered efficiently by modifying the normal strain in Eq. (2)

$$\mathbf{F}_n^{cohe} = M_n^{cohe} A (\varepsilon_n - \alpha \Delta T) \mathbf{n}. \quad (9)$$

Up to now, two effects of temperature change on DEM have been carefully treated by changing the particle size and modifying normal cohesive force.

2.2. Lattice Boltzmann method

For heat conduction process, temperature distribution can be determined by solving the energy equation. Without heat source term, it is written as

$$\rho c_p \left(\frac{\partial T}{\partial t} \right) = k \nabla^2 T, \quad (10)$$

where ρ is the density, k is the thermal conductivity, and c_p is the specific heat capacity. In current model, Eq. (10) is solved by lattice Boltzmann method (LBM), which is intrinsically a mesoscopic approach based on the evolution of statistic distribution of lattices, and the obtained macroscopic variables (i.e. T) obey the required governing equations (i.e. Eq. (10)) (Wang et al., 2007). It has achieved considerable success in simulating fluid flow (Chen and Doolen, 1998; Wang et al., 2016) and associated transport phenomenon (He et al., 2017) especially for complex geometry boundary conditions. Recently, LBM has been coupled with DEM to simulate the hydro-mechanical coupled process such as sand production (Chen et al., 2016) and hydraulic fracture (Chen and Wang, 2017) owing to its accurate calculation of hydraulic force. The basic variable in LBM is distribution function g , and its evolution equation (D3Q7) is given as

$$g_\alpha(\mathbf{r} + \mathbf{e}_\alpha \delta_t, t + \delta_t) - g_\alpha(\mathbf{r}, t) = -\frac{1}{\tau} [g_\alpha(\mathbf{r}, t) - g_\alpha^{eq}(\mathbf{r}, t)], \quad (11)$$

where \mathbf{r} is the location vector, t is the real time, δ_t is the time step, and g_α^{eq} is the equilibrium distribution of distribution function g_α

$$g_\alpha^{eq} = \begin{cases} \frac{T}{4}, & \alpha = 0 \\ \frac{T}{8}, & \alpha = 1 - 6 \end{cases}, \quad (12)$$

\mathbf{e}_α is the discrete velocity

$$\mathbf{e}_\alpha = \begin{cases} (0, 0, 0) & \alpha = 0 \\ (\pm 1, 0, 0)c, (0, \pm 1, 0)c, (0, 0, \pm 1)c & \alpha = 1 - 6 \end{cases}, \quad (13)$$

where $c = \delta_x / \delta_t$, δ_x is the grid size. Parameter τ is the dimensionless relation time determined by the thermal conductivity

$$\tau = \frac{1}{2} + \frac{4k\delta_t}{\rho c_p \delta_x^2}. \quad (14)$$

The macroscopic variables temperature and heat flux are calculated as

$$T = \sum_{\alpha} g_{\alpha}, \quad (15)$$

$$\mathbf{q} = \left(\sum_{\alpha} c_{\alpha} g_{\alpha} \right) \frac{\tau - 0.5}{\tau}. \quad (16)$$

During thermo-mechanical coupled simulation, a set of LBM grids are defined as background lattices to calculate temperature distribution (using Eq. (11)) in rock sample at each time step. Then the lattice information (temperature) is projected to the DEM particle to determine its temperature change, which is calculated by averaging the temperature at the nodes inside the DEM particle. With the temperature change, DEM particle expansion is achieved by changing the radius of erosion sphere (using Eq. (8)). These above steps are repeated until the simulation is finished.

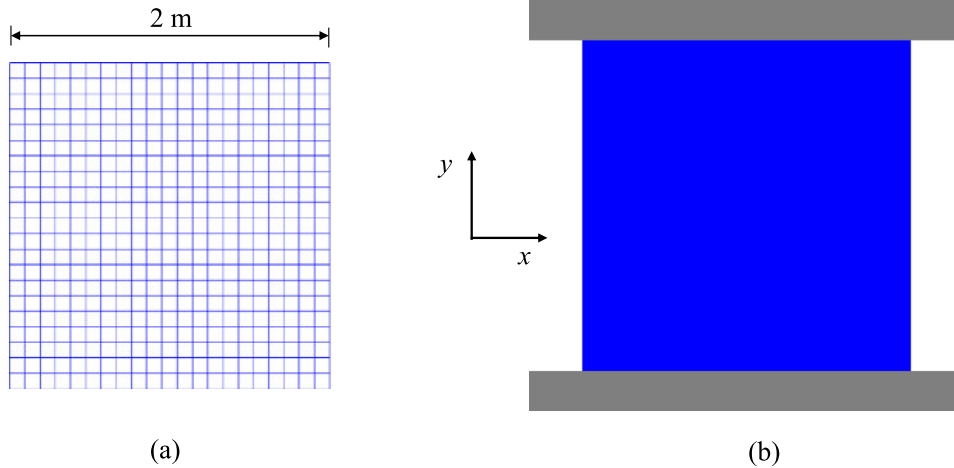


Fig. 4. Benchmark cases for uniformly heated specimens, (a) free expansion of a uniformly heated specimen, (b) constrained expansion of a uniformly heated specimen.

Table 1

Numerical results for free expansion of a uniformly heated specimen.

	x direction	y direction
Analytical solution	3.00×10^{-4}	3.00×10^{-4}
Numerical results	3.02×10^{-4}	3.02×10^{-4}
Deviation	0.67%	0.67%

3. Validations

In this part, current thermo-mechanical coupled model is validated by some benchmark cases, which include free expansion of a uniformly heated specimen, constrained expansion of a uniformly heated specimen, and constrained expansion of a specimen with heat conduction.

3.1. Free expansion of a uniformly heated specimen

The first benchmark is the free expansion of a square specimen with unconstrained boundaries. In order to compare with analytical solutions for isotropic and homogeneous elastic material, the square specimen is discretized as a collection of 441 sphero-squares (see Fig. 4(a)). Initially, a uniform temperature change ΔT is applied to the square specimen with thermal expansion coefficient α . At the equilibrium state, analytical solution for the thermal strain is given by

$$\varepsilon_x = \varepsilon_y = \alpha \Delta T. \quad (17)$$

In this simulation, thermal expansion coefficient of the specimen is set as $3 \times 10^{-6} \text{ } ^\circ\text{C}^{-1}$, and the temperature change is $100 \text{ } ^\circ\text{C}$. Numerical results of thermally induced strain in x and y direction are presented in Table 1, which agree well with the analytical ones.

3.2. Constrained expansion of a heated specimen

In the second case, a uniform temperature change ΔT is also applied to the square specimen same as that in Section 3.1, but here the specimen is constrained in y direction (see Fig. 4(b)). Thus, it can only expand free in x direction, and thermal stress is induced in y direction. In current simulation, the constrained boundary condition is achieved by fixing the position of the upper and lower layer of DEM particles in y direction (see Fig. 4(a)), but they can move free in x direction. It should be noted that the gray plates in Fig. 4(b) are just used to show the constrained boundary condition in y direction, which do not exist in the simulation. In this case, the thermally induced stress in y direction is analytically given by

$$\sigma_y = \alpha \Delta T E, \quad (18)$$

where E is the Young's modulus of the specimen.

For current square specimen, Young's modulus E is numerically measured by uniaxial compression test, which is 13.3 GPa. With temperature change $\Delta T = 100 \text{ } ^\circ\text{C}$, thermal expansion coefficient $\alpha = 3.0 \times 10^{-6} \text{ } ^\circ\text{C}^{-1}$, using the measured Young's modulus $E = 13.3 \text{ GPa}$, the analytical solution of thermal stress $\sigma_y = 3.99 \text{ MPa}$. Numerical thermal stress in y direction is presented in Fig. 5, and the agreement is good.

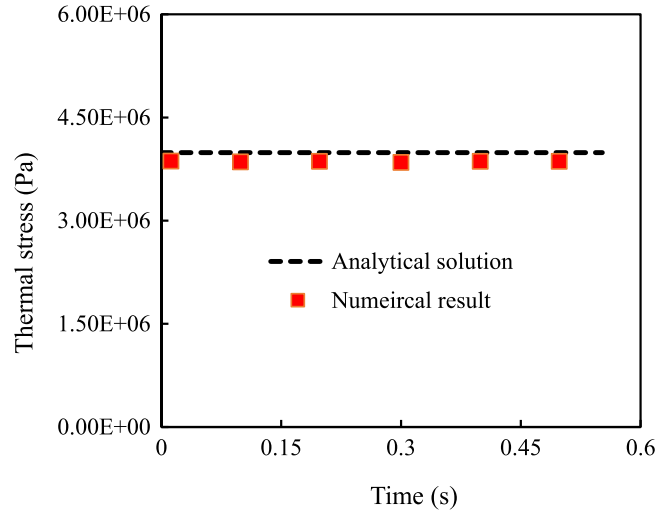


Fig. 5. Numerical result of thermal stress in y direction caused by the constrained expansion of a heated specimen, which agrees well with the analytical solution.

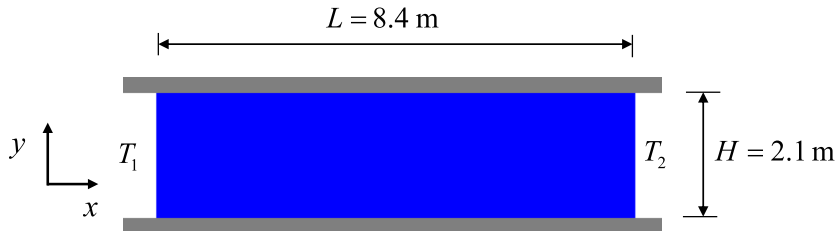


Fig. 6. Physical model for heat conduction in a rectangular specimen (blue part) with constant temperature T_1 and T_2 at left and right boundaries, respectively. The upper and lower boundaries are insulated. The rectangular specimen is constrained in y direction, so it can only expand free in x direction and thermal stress is induced in y direction. (For interpretation of the references to colour in this figure legend, the reader is referred to the web version of this article.)

3.3. Constrained expansion of a specimen with heat conduction

In above cases, temperature distribution is uniform in the specimen, so no heat conduction occurs. In this part, heat conduction in a constrained specimen is simulated, where two boundary conditions for heat conduction, constant temperature and constant heat flux, are considered, respectively.

3.3.1. Constant temperature boundary condition

Heat conduction in a rectangular specimen with length $L = 8.4$ m and height $H = 2.1$ m is simulated (see Fig. 6). Initially, a uniform temperature of 100 °C is distributed in the sample. Then the left boundary is exposed to a constant temperature of $T_1 = 400$ °C, while the right boundary is kept at a constant temperature of $T_2 = 100$ °C. The upper and lower boundaries are insulated. Similarly to Section 3.2, the rectangular specimen is also constrained in y direction, where the lower and upper layer of DEM particles in the specimen are mechanically fixed in y direction and free in x direction.

Under the above boundary conditions, the temperature distribution in y direction is same, which only varies along x direction, so it can be simplified as a one-dimensional heat conduction process and mathematically described as

$$\frac{\partial T}{\partial t} = \frac{k}{\rho c_p} \frac{\partial^2 T}{\partial x^2}, \quad (19)$$

$$\begin{cases} T = 100 \text{ °C}, & 0 < x < 8.4 \text{ m}, & t = 0 \\ T = T_1 = 400 \text{ °C}, & x = 0 \\ T = T_2 = 100 \text{ °C}, & x = 8.4 \text{ m} \end{cases}, \quad (20)$$

where thermal conductivity $k = 3.5$ W/mK, density $\rho = 2600$ kg/m³, specific heat capacity $c_p = 1015$ J/kgK.

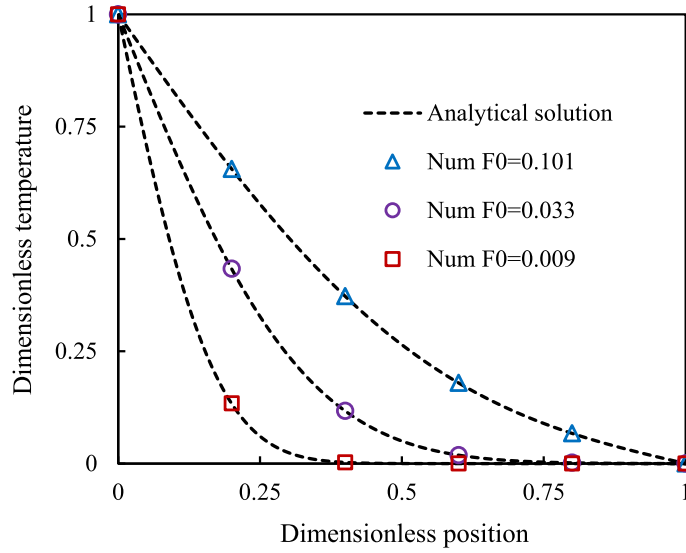


Fig. 7. Comparison between numerical dimensionless temperature distribution along x direction with analytical solutions, and the agreement is good, which shows the reliability of current LBM code for solving heat transfer process.

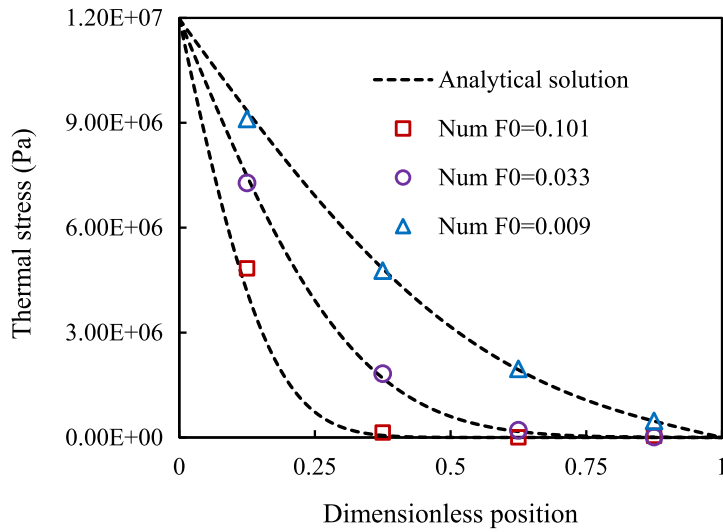


Fig. 8. Comparison between numerical thermal stress along x direction with analytical solutions, and the agreement is good, which shows current model successfully simulates the thermo-mechanical coupled process with heat conduction.

By introducing the dimensionless spatial and temporal coordinates as: $X = x/L$ and $F_0 = (tk)/(\rho c_p L^2)$, the analytical dimensionless temperature is given by

$$\Theta = \frac{T(x, t) - T_2}{T_1 - T_2} = 1 - X - \frac{2}{\pi} \sum_{n=1}^{\infty} \frac{\sin(n\pi X)}{n} \exp[-(n\pi)^2 F_0]. \tag{21}$$

Fig. 7 compares the current numerical dimensionless temperature distribution with analytical one at different dimensionless instants, and good agreement is obtained, which confirms the reliability of current LBM code for solving heat transfer process.

When the temperature distribution in the specimen is calculated, thermal stress induced by the temperature change is analytically given by

$$\sigma_y = \alpha E \Delta T, \tag{22}$$

where $E = 13.3$ GPa as in Section 3.2, ΔT is the temperature change. The numerical thermal stress along x direction is plotted in Fig. 8, which agrees well with the analytical solution.

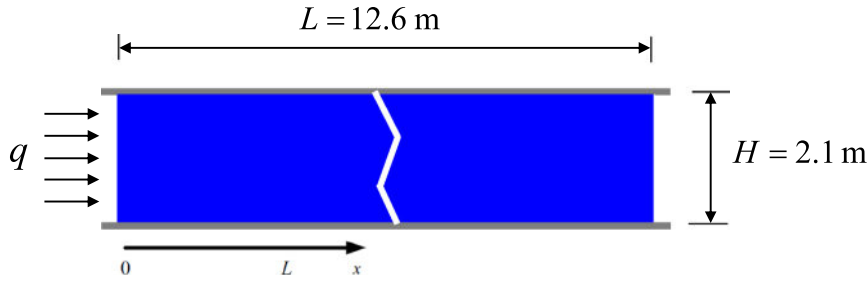


Fig. 9. Physical model for heat conduction in a rectangular specimen (blue part) with constant heat flux q applied in the left boundary. The upper and lower boundaries are insulated. The rectangular specimen is constrained in y direction, so it can only expand free in x direction and thermal stress is induced in y direction. (For interpretation of the references to colour in this figure legend, the reader is referred to the web version of this article.)

3.3.2. Constant heat flux boundary condition

Heat conduction in a constrained thin specimen with constant heat flux is simulated in this part (see Fig. 9). The length and width of the specimen is 12.6 m and 2.1 m, respectively. Initially, the uniform temperature in the specimen is 0 °C. Then a constant heat flux $q = 100 \text{ W/m}^2$ is applied at the left boundary. Upper and lower boundaries are insulated. This process can also be treated as a one-dimensional problem and described mathematically as

$$\frac{\partial T}{\partial t} = \frac{k}{\rho c_p} \frac{\partial^2 T}{\partial x^2}, \quad (23)$$

$$\begin{cases} T = 0, 0 < x < 12.6 \text{ m}, t = 0 \\ q = 100 \text{ w/m}^2, x = 0 \end{cases}. \quad (24)$$

Before the temperature change happens at the right boundary of the specimen, the analytical solution for temperature distribution within the semi-infinite solid can be applied to this situation. Temperature $T(x, t)$ as a function of the distance from the left boundary x and time t is written as

$$T(x, t) = \frac{2q}{k} \left[\left(\frac{\kappa t}{\pi} \right)^{1/2} \exp\left(\frac{-x^2}{4t\kappa}\right) - \frac{x}{2} \operatorname{erfc}\left(\frac{x}{2\sqrt{\kappa t}}\right) \right], \quad (25)$$

where κ is the thermal diffusivity given by

$$\kappa = \frac{k}{\rho c_p}. \quad (26)$$

Temperature distribution in the specimen along x direction at different dimensionless time ($F_0 = (tk)/(\rho c_p L^2)$) is presented in Fig. 10(a), which agrees well with analytical solutions. Similar to the above cases, the specimen is also constrained in y direction. The induced thermal stress in y direction is numerically measured and compared with the analytical solutions calculated by Eq. (22), and the agreement is also good (see Fig. 10(b)).

The above benchmark cases indicate that the proposed thermo-mechanical coupled DEM model can efficiently deal with heat conduction and thermally-induced deformation problems.

4. Thermal gradient cracking simulation

For further validation of current model, thermal gradient cracking is considered, which may happen in geological storage of nuclear waste. In nuclear waste repository, the heat caused by the decay of radioactive substance increases the surrounding rock. This temperature rise will induce the thermal cracking in rock via two mechanisms (Jansen et al., 1993). First, temperature gradient can lead to the internal constraint for thermal expansion and hence induce the thermal stress for crack formation (thermal gradient cracking), when it exceeds the local strength of rock (Ishida et al., 2005; Jansen et al., 1993). Second, heterogeneity is a typical feature of rock (Ma et al., 2011) owing to its various mineral components with different thermal expansion coefficients (Cho et al., 2007). Thus, thermal expansion mismatch between adjacent crystalline grains can also result in the sufficient thermal stress to crack the rock even with the uniform temperature change (Johnson et al., 1978; Zhao, 2016).

Therefore, temperature gradient and rock heterogeneity are two main factors affecting the thermally induced damage in rock, and one critical question should be addressed is: what is the role of rock heterogeneity in thermal gradient cracking process? It is helpful to select a proper formation for minimizing thermally induced damage. However, the above two mechanisms are coupled with each other, and little knowledge is known about its effect on the final damage.

Recently, some researchers have simulated thermal gradient cracking in rock using DEM (Wanne and Young, 2008; Xia et al., 2014; Zhao, 2016), but all of them are based on spherical particles, which cannot capture all the consequences of real

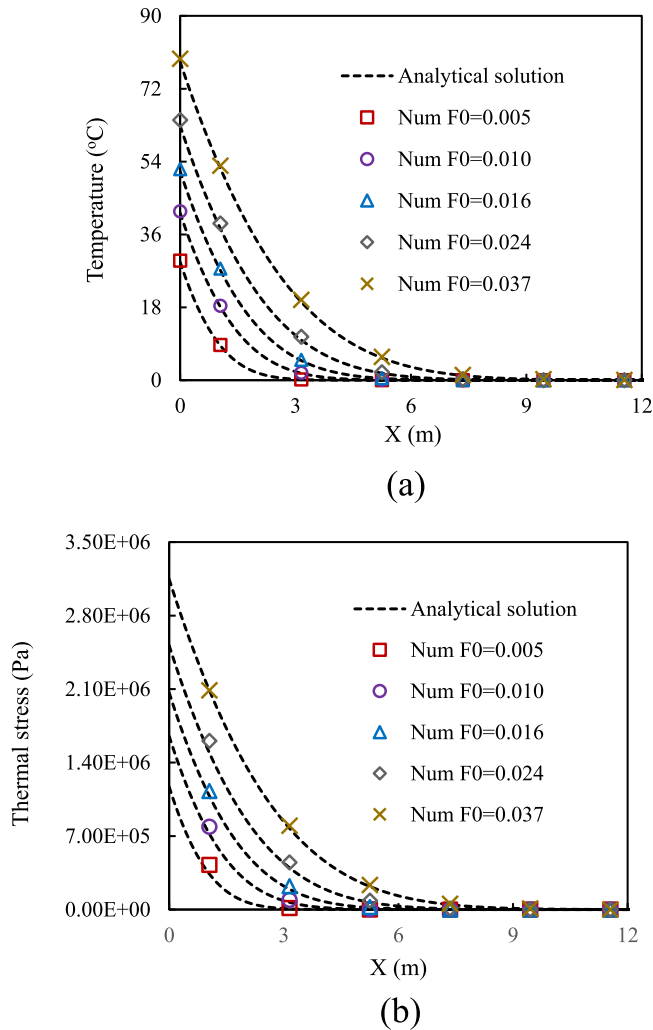


Fig. 10. Comparison of numerical results with the corresponding analytical solutions at different dimensionless time F_0 , (a) temperature and (b) thermal stress distribution along x direction.

rock composed of irregular grains (e.g. granite) just as presented in Section 1. In this study, current thermo-mechanical coupled model is used to explore the thermal gradient cracking of rock, and the specific emphasis is put on rock heterogeneity effect on this process.

4.1. DEM model calibration

In continuum-based methods, the input properties (e.g. Young's modulus E , compressive strength σ_c , tensile strength σ_t etc.) can be directly obtained from measurements performed on laboratory specimens. In discrete element method (DEM), microscopic rather than macroscopic properties are the basic parameters, which cannot be obtained directly from laboratory experiments (Potyondy and Cundall, 2004). Thus, in order to simulate a specific material, calibration process is needed to determine the microscopic parameters.

Here, granite is used to calibrate current DEM model, which is a promising material for nuclear waste disposal owing to its high strength and low permeability (Kim et al., 2011). As the first step, two material tests, uniaxial compression test and Brazilian test, are simulated at uniform room temperature ($20\text{ }^{\circ}\text{C}$) to obtain the microscopic parameters in DEM, and with these parameters the macroscopic properties of granite measured under the same condition (at room temperature $20\text{ }^{\circ}\text{C}$) can be reproduced within a reasonable range. In this work, no further efforts were made to match the very exact values of granite macro properties. We can do this here because our object is to show the ability of current DEM to capture the high value of strength ratio (σ_c/σ_t), which is an important characteristic of rock but greatly underestimated by previous DEM using spherical elements (Scholtès and Donzé, 2013).

Table 2
Microscopic parameters in current DEM for granite.

Parameter	Value
Normal spring stiffness K_n	$1.0 \times 10^8 \text{ N/m}$
Tangential spring stiffness K_t	$1.0 \times 10^8 \text{ N/m}$
Normal elastic modulus M_n^{cohe}	$2.0 \times 10^9 \text{ Pa}$
Tangential elastic modulus M_n^{cohe}	$4.17 \times 10^9 \text{ Pa}$
Bonding strength threshold ε_{th}	0.024
Time step Δt	$1.2 \times 10^{-7} \text{ s}$

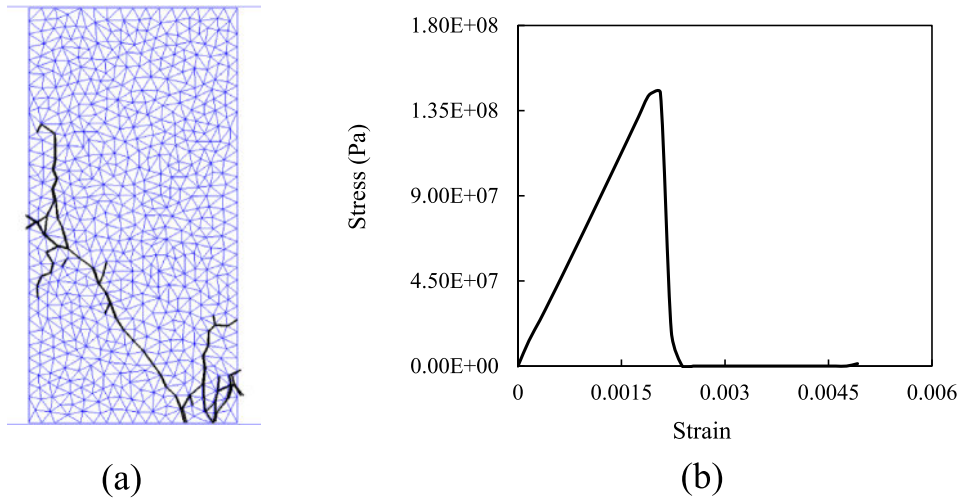


Fig. 11. Typical results for uniaxial compression test, (a) damage pattern and (b) stress-strain response obtained from current simulation, and according to the stress-strain response Young's modulus E and compressive strength σ_c can be obtained.

Table 3
Macroscopic parameters obtained from DEM and experiments.

	Young's modulus		Compressive strength σ_c		Tensile strength σ_t		σ_c/σ_t Value
	Value /GPa	Relative error	Value /MPa	Relative error	Value /MPa	Relative error	
Sphere DEM	70.9	2.8%	199.1	0.45%	44.7	380.6%	4.45
Current DEM	75	8.6%	145	27.5%	10.2	9.6%	14.21
Experiment	69 ± 5.8		200 ± 22		9.3 ± 1.3		21.5

When the temperature changes, macro properties of rock may vary. The formation of micro cracks induced by thermal stress is regarded as a most important reason for this rock property variation (David et al., 1999; Zhao, 2016). Unlike continuum-based methods that utilizes average measures of rock degradation in constitutive equations, discrete element method, as a micro scale method, is expected to automatically capture this macro property variation with temperature owing to its explicit representation of damage development in rock (Zhao, 2016).

Current DEM for granite is described by the microscopic properties in Table 2. These parameters are chosen to match the macroscopic properties of granite. Typical stress-strain response and damage behavior in uniaxial compression test are shown in Fig. 11, where the specimen (20 cm in height and 10 cm in width) is discretized into a collection of triangular particles. According to the stress-strain response (Fig. 11(b)), Young's modulus E and compressive strength σ_c can be obtained, which are listed in Table 3 and compared with experimental values.

A common method used to measure the tensile strength of brittle material (e.g. rock) is Brazilian test (Jaeger and Hoskins, 1966), where a disc sample is compressed along the direction parallel to its diameter. Here, Brazilian test is also simulated to obtain the tensile strength of current DEM model with microscopic parameters in Table 2, where the radius of the disc is 10 cm. The failure behavior and force of the loading plate during compression are presented in Fig. 12. Fig. 12(a) shows that the disc is split into two halves along the diameter, which is a typical feature in Brazilian test (Li and Wong, 2013). In addition, according to the F_{max} in Fig. 12(b), the tensile strength σ_t of the specimen (with diameter D and thickness T) can be obtained (Li and Wong, 2013)

$$\sigma_t = \frac{2F_{max}}{\pi DT}, \quad (27)$$

which is also listed in Table 3.

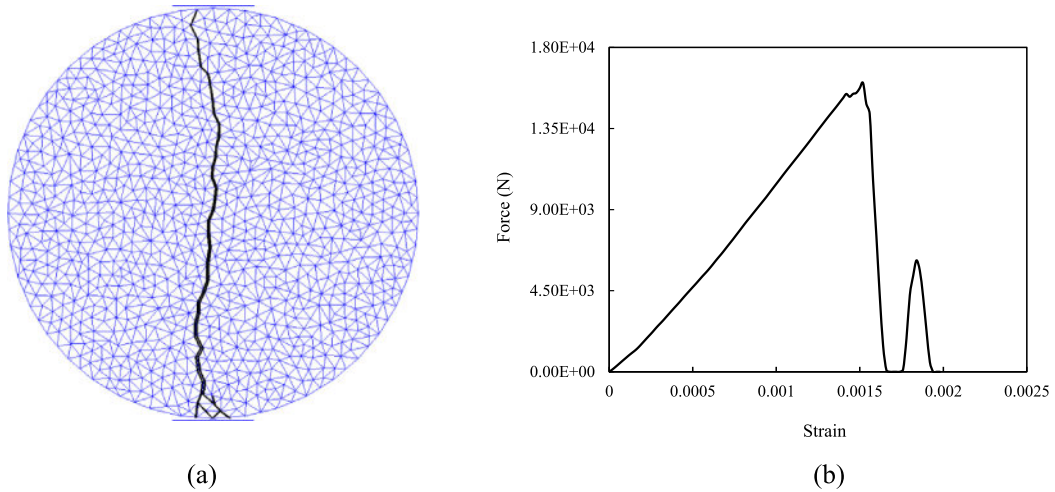


Fig. 12. Typical results for Brazilian test, (a) damage pattern and (b) force applied on loading plate during compression process, where the F_{max} can be used to determine tensile strength σ_t of the specimen.

Table 3 shows the macroscopic properties simulated with current DEM, and the results obtained from spherical particles based DEM (Potyondy and Cundall, 2004) are also listed for comparison. The experimental values are from Lac du Bonnet granite (Potyondy and Cundall, 2004), which is often cited as a reference for modeling brittle rock. It can be seen that current model can provide reasonable values for both tensile strength and compressive strength. It is because the ratio of compressive to tensile strength (σ_c/σ_t) in current model is much closer to the experimental one. Indeed, whatever the microscopic parameters are used, high ratio between compressive strength and tensile strength (σ_c/σ_t) cannot be obtained in spherical particles based DEM (Scholtès and Donzé, 2013). Therefore, in the framework of spherical particles based DEM, the researchers only calibrate the compressive strength, which results in a much high over prediction of tensile strength (Potyondy and Cundall, 2004; Wanne and Young, 2008; Zhao, 2016).

4.2. Physical model for thermal gradient cracking

In order to investigate the thermally induced damage process involved in nuclear waste disposal, some techniques (e.g. ultrasonic imaging and acoustic emission monitoring technique) were developed to identify the cracks in larger-scale laboratory samples and explore the thermal fracturing due to temperature gradient (Ishida et al., 2005; Jansen et al., 1993). In these experiments, an unconfined cubic sample with a central vertical borehole is considered, and a cartridge heater is placed in the borehole to induce temperature gradient in the rock. As a result, a macro fracture is observed, which initiates at the outer edge of the sample and then propagates inward, until intersecting the central borehole (Jansen et al., 1993).

This experiment is simulated using current thermo-mechanical coupled model, and the focus is paid on the heterogeneity effect on this process. The physical model is presented in Fig. 13, where an unconfined square rock specimen (a side length of 30 cm) with a central borehole (a diameter of 3.15 cm) is considered. The rock specimen is discretized as a collection of bonded triangular particles. The initial temperature of the rock specimen is 20 °C. During the simulation, the temperature in the center point (red point in Fig. 13(a)) increases gradually, while the temperature on the outer sides are fixed at 20 °C, which results in the temperature gradient and thereby the thermal stress in the specimen. When the thermal stress exceeds the local strength, thermally induced damage happens. Temperature distribution is calculated on the background regular lattices using LBM (see Fig. 13(a)), and the temperature in each triangular particle can be determined by averaging the temperatures at the grids inside it.

In order to consider the heterogeneity effect, two specimens with same mesh morphology are considered, homogeneous (Fig. 13(c)) and heterogeneous one (Fig. 13(d)). The mechanical properties in homogeneous and heterogeneous specimens are same that are listed in Table 2. The heterogeneous sample is uniform in texture and its composition consists of on average of 37.9 % quartz, 55.8 % feldspar, and 6.3 % mica mineral according to the analysis of digital image of granite (Yu et al., 2015). Their thermal expansion coefficients are equal to $11 \times 10^{-6} \text{ }^\circ\text{C}^{-1}$, $6 \times 10^{-6} \text{ }^\circ\text{C}^{-1}$ and $3 \times 10^{-6} \text{ }^\circ\text{C}^{-1}$, respectively (Yu et al., 2015). In homogeneous specimen, the same thermal expansion coefficient $7.7 \times 10^{-6} \text{ }^\circ\text{C}^{-1}$ is assigned to all the triangular particles, which equals to the average one in heterogeneous specimen. The values of $1015 \text{ Jkg}^{-1} \text{ }^\circ\text{C}^{-1}$, 2650 kg/m^3 and $3.5 \text{ Wm}^{-1} \text{ }^\circ\text{C}^{-1}$ are used for the specific heat capacity, density and thermal conductivity respectively for all triangular particles in both heterogeneous and homogeneous specimens.

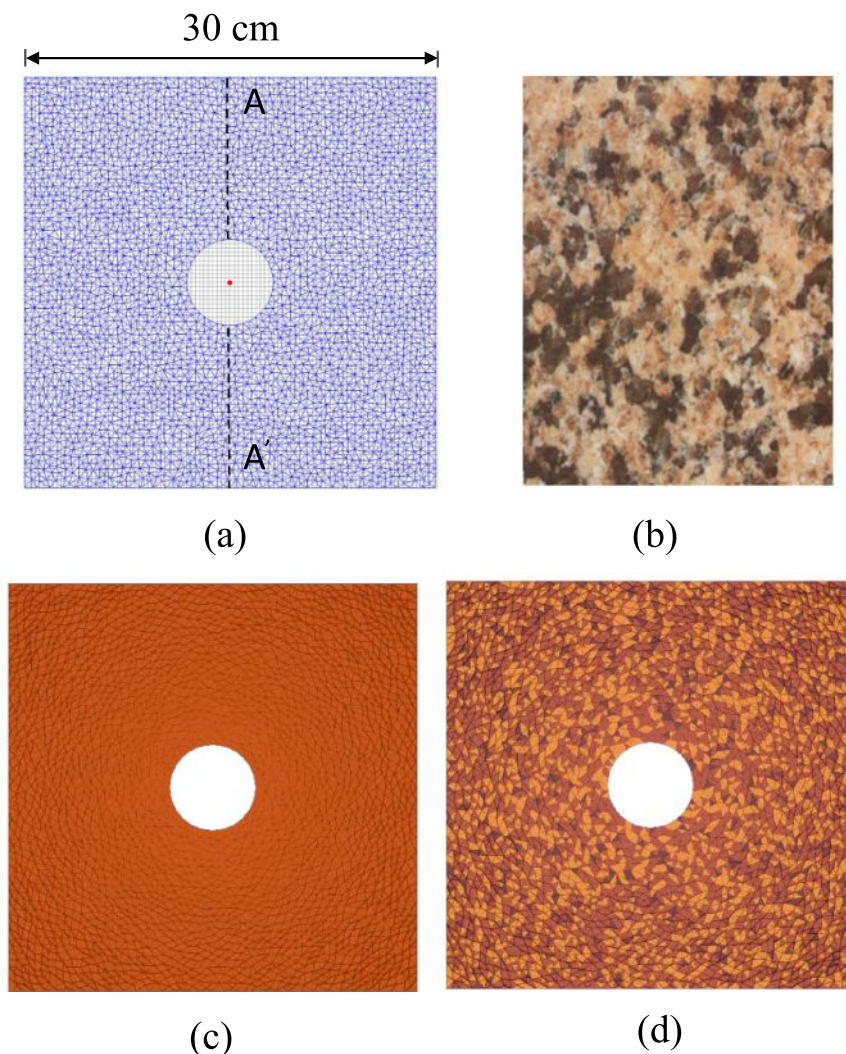


Fig. 13. Physical model used for thermal gradient cracking simulation. (a) Rock specimen with a borehole in the center is discretized as a collection of bonded triangular particles. (b) Lau du Bonnet granite (Cho et al., 2007). (c) Homogeneous and (d) heterogeneous samples considered in current simulation. (For interpretation of the references to colour in this figure legend, the reader is referred to the web version of this article.)

4.3. Heterogeneity effect

Temperature gradient induced macroscopic fracture evolution is presented in Fig. 14, which shows that the damage process can be divided into two stages in both homogeneous and heterogeneous specimens. In the first stage, a macro fracture initiates from the outer side of the specimens and then propagates inwards until reaches the surface of the borehole. In the second stage, another fracture propagates from the borehole to the opposite lateral edge of the sample. The fracture propagation path obtained from numerical simulation agrees well with the experimental observations, as shown in Fig. 14(c) (Ishida et al., 2005).

Although the macroscopic fracture propagation pattern is similar in homogeneous and heterogeneous specimens, some differences still exist. In homogeneous one, macroscopic fracture induced by the temperature gradient dominates the fracturing behavior. However, in heterogeneous specimen, more micro cracks scattering uniformly around the borehole are observed, which account for a large part of final damage. Fig. 15 shows the variation of micro cracks (broken bond number) with temperature at surface of the borehole in homogeneous and heterogeneous specimens. When the temperature at the borehole surface reaches one critical value, micro cracks increase rapidly and thermally induced damage happens. This critical value in heterogeneous specimen is smaller than that in homogeneous one, which means thermal damage is more easily induced in heterogeneous specimen owing to the stress concentration in the mineral with high thermal expansion coefficient. In addition, under the same temperature gradient more cracks are observed in heterogeneous sample, which corresponds to a more serious damage.

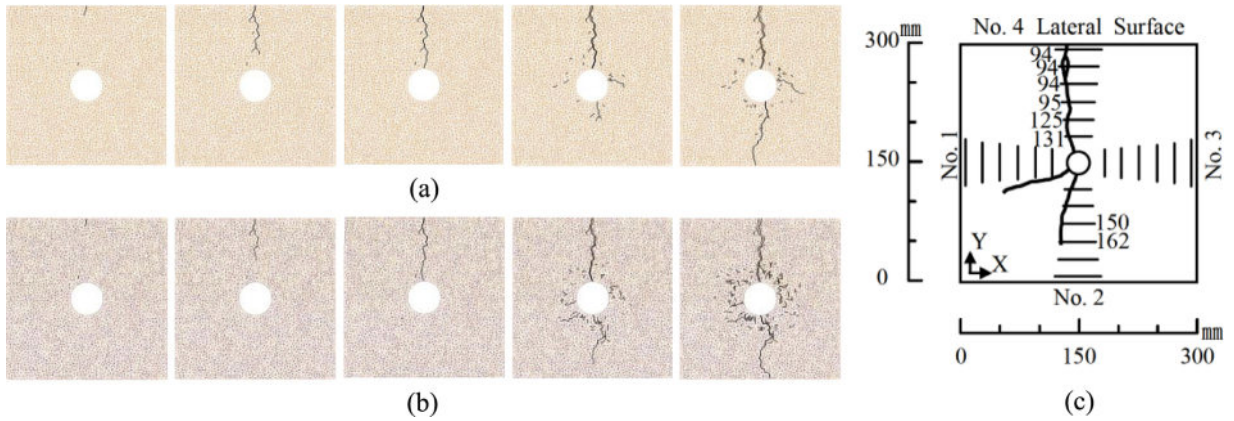


Fig. 14. Temperature gradient induced fracture evolution obtained from current simulation in (a) homogeneous and (b) heterogeneous specimens. (c) Thermal crack extension observed in experiment (Ishida et al., 2005), which is indicated by the voltage drops of the electro-conductive paint in the specimen.

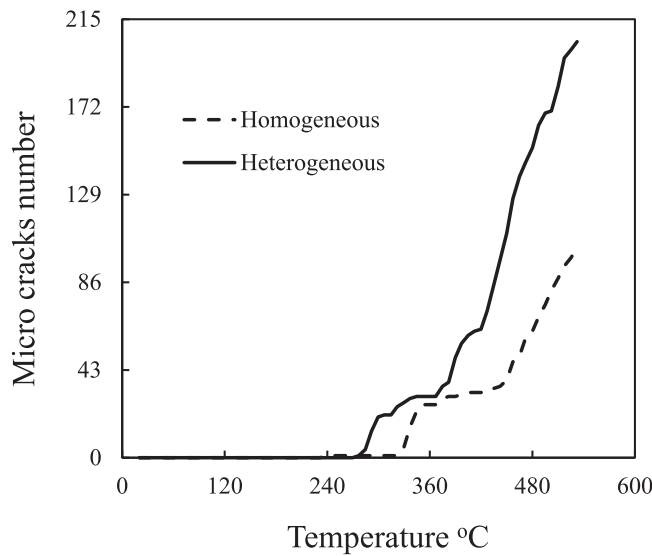


Fig. 15. Micro cracks evolution in homogeneous and heterogeneous specimens during thermal gradient cracking simulation, which shows that damage is more serious in heterogeneous specimen under the same condition.

In order to explain the above phenomena, tensile force between triangular particles along cross section A-A' (see Fig. 13(a)) before cracking is shown in Fig. 16. In both homogeneous and heterogeneous specimens, tensile force caused by the temperature gradient increases monotonously with the distance to the borehole center, which is consistent with the traditional theory (Jansen et al., 1993). Thus, maximum tensile force occurs at the outer edge of the sample. As a result, the macroscopic fracture initiates at the outside of the sample and then propagates inwards. However, in heterogeneous sample, tensile force around the borehole is larger than that in homogeneous one (see Fig. 16(c)). This is because in heterogeneous sample, besides temperature gradient, thermal expansion mismatch can also induce thermal stress, which increases with temperature change. In current simulation, the temperature change around the borehole is highest, so the thermal stress caused by thermal expansion mismatch in this region is larger than that in other parts, which induces more uniformly scattered micro cracks around the borehole in the heterogeneous sample.

Current simulation shows that rock heterogeneity has a great effect on thermal gradient cracking process, which results in more serious damage in heterogeneous specimen especially in the region with high temperature change. For geological storage of nuclear waste, the temperature change of rock near the nuclear waste is higher, so more cracks may be induced around the repository if a highly heterogeneous formation is selected, which greatly increases the risk of nuclear leakage. Thus, homogenous formation is suggested for nuclear waste disposal if other parameters are same.

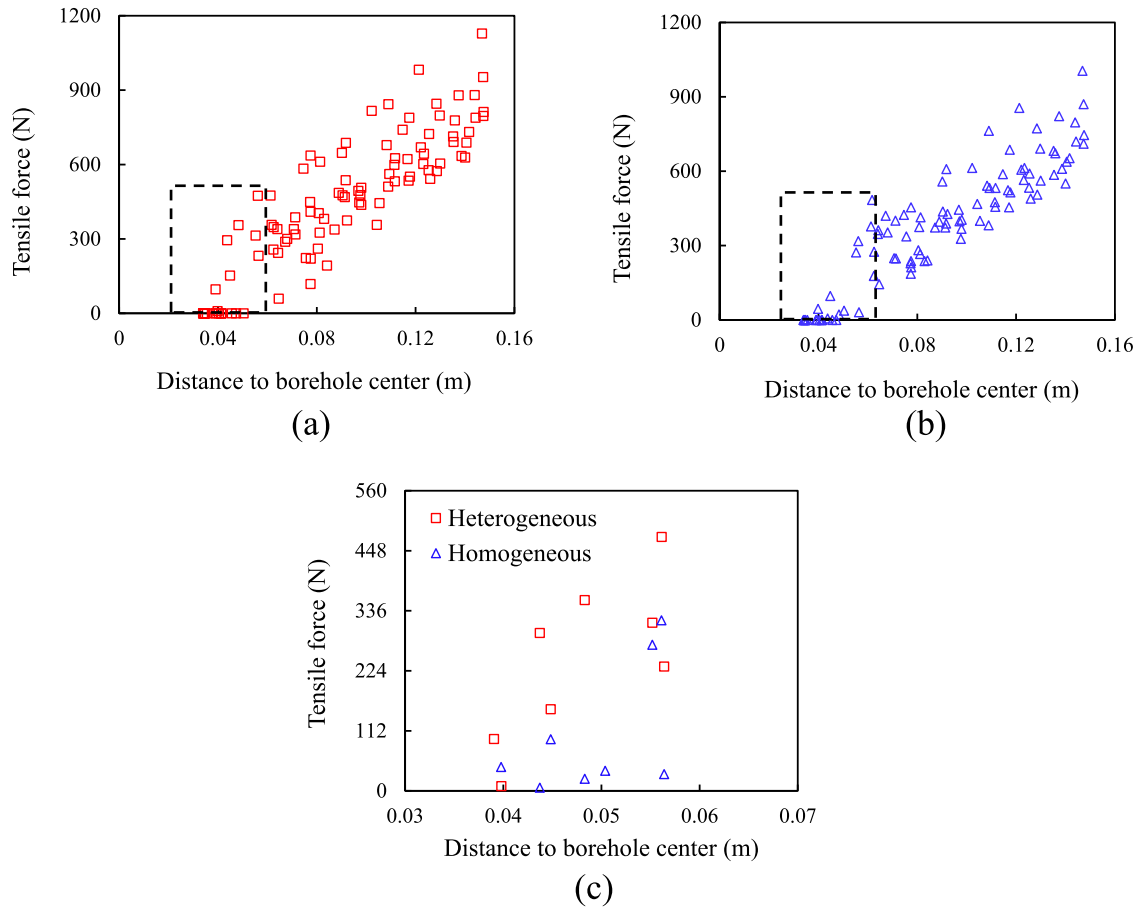


Fig. 16. Tensile force between triangular particles along cross section A-A' in (a) heterogeneous and (b) homogenous specimens. (c) Comparison of tensile force around borehole in homogeneous and heterogeneous specimens.

5. Conclusions

We have presented a thermo-mechanical coupled model combining discrete element method (DEM) for solid deformation, fracturing behavior and lattice Boltzmann method (LBM) for heat transfer to mimic thermally induced damage in rock. Current model is based on the framework of discrete sphero-polyhedra element method (DSEM), which allows to deal with grains of complex shapes and hence can more accurately capture the fundamental aspects of brittle rock behavior such as high ratio of compressive to tensile strength. In addition, in current model non-spherical particle size change caused by the temperature change can be easily achieved in algorithm by changing the radius of erosion sphere, which greatly improves the computation efficiency. In order to validate the proposed model, some benchmark cases are considered, for which analytical solutions are available. The agreement between numerical results and analytical solutions is good, which demonstrates that current model can be further used to explore the underlying physics involved in the thermo-mechanical coupled process.

Furthermore, thermal gradient cracking, which may happen in nuclear waste disposal, is simulated with an emphasis on heterogeneity effect on this process. Present model successfully captures the feature of thermal gradient cracking observed in experiments that fracture initiates from the outer side of the sample and then propagates inwards. Current numerical results show that rock heterogeneity has a great effect on thermal gradient cracking, and the damage is more easily and seriously induced in heterogeneous rock. It may provide some implications for nuclear waste disposal that homogenous formation is suggested to store nuclear waste.

The success of the reproduction of the thermal gradient cracking evolution indicates that current model can be applied to other thermo-mechanical coupled processes in rock. Therefore, present work provides a promising approach to explore the mechanism of thermally induced damage of rock involved in some geologic applications such as geothermal exploration and hydraulic fracture stimulation.

Acknowledgments

This work is financially supported by the NSFC -DFGgrant (No. 11761131012) and National Science and Technology Major Project on Oiland Gas (No.2017ZX05013001). The authors want to acknowledge the open source library MechSys developed by S. A. Galindo Torres (<http://mechsys.nongnu.org/index.shtml>).

Supplementary materials

Supplementary material associated with this article can be found, in the online version, at doi:10.1016/j.jmps.2018.03.023.

References

- AbuAisha, M., Loret, B., Eaton, D., 2016. Enhanced geothermal systems (EGS): hydraulic fracturing in a thermo-poroelastic framework. *J. Petrol. Sci. Eng.* 146, 1179–1191.
- Barron, R.F., Barron, B.R., 2011. *Design for Thermal Stresses*. John Wiley & Sons.
- Behraftar, S., Torres, S.G., Scheuermann, A., Williams, D., Marques, E., Avarzaman, H.J., 2017. A calibration methodology to obtain material parameters for the representation of fracture mechanics based on discrete element simulations. *Comput. Geotech.* 81, 274–283.
- Bierwisch, C., Kraft, T., Riedel, H., Moseler, M., 2009. Three-dimensional discrete element models for the granular statics and dynamics of powders in cavity filling. *J. Mech. Phys. Solids* 57 (1), 10–31.
- Chen, S., Doolen, G.D., 1998. Lattice Boltzmann method for fluid flows. *Annu. Rev. Fluid Mech.* 30 (1), 329–364.
- Chen, Z., Wang, M., 2017. Pore-scale modeling of hydromechanical coupled mechanics in hydrofracturing process. *J. Geophys. Res. Solid Earth* 122 (5), 3410–3429.
- Chen, Z., Xie, C., Chen, Y., Wang, M., 2016. Bonding strength effects in hydro-mechanical coupling transport in granular porous media by pore-scale modeling. *Computation* 4 (1), 1–15.
- Chen, Z.Q., Yang, Z., Wang, M., 2018. Hydro-mechanical coupled mechanisms of hydraulic fracture propagation in rocks with cemented natural fractures. *J. Petrol. Sci. Eng.* 163, 421–434.
- Cho, N., Martin, C., Segol, D., 2007. A clumped particle model for rock. *Int. J. Rock Mech. Min. Sci.* 44 (7), 997–1010.
- Cundall, P.A., Strack, O.D., 1979. A discrete numerical model for granular assemblies. *Geotechnique* 29 (1), 47–65.
- David, C., Menéndez, B., Darot, M., 1999. Influence of stress-induced and thermal cracking on physical properties and microstructure of La Peyratte granite. *Int. J. Rock Mech. Min. Sci.* 36 (4), 433–448.
- Galindo-Torres, S., Munoz, J., Alonso-Marroquin, F., 2010. Minkowski-Voronoi diagrams as a method to generate random packings of spheropolygons for the simulation of soils. *Phys. Rev. E* 82 (5), 056713.
- Galindo-Torres, S., Pedrosa, D., Williams, D., Li, L., 2012. Breaking processes in three-dimensional bonded granular materials with general shapes. *Comput. Phys. Commun.* 183 (2), 266–277.
- He, X., Guo, Y., Li, M., Pan, N., Wang, M., 2017. Effective gas diffusion coefficient in fibrous materials by mesoscopic modeling. *Int. J. Heat Mass Tran.* 107, 736–746.
- Heard, H., 1989. Thermal stress cracking in granite. *J. Geophys. Res.* 94 (B2), 1745–1758.
- Ishida, T., Suemune, K., Fukui, H., Kinoshita, N., 2005. Effect of thermal stress in fracturing by expansive cement agent in comparison with a borehole pressurizing test and a heater test. The 40th US Symposium on Rock Mechanics (USRMS).
- Jaeger, J., Hoskins, E., 1966. Rock failure under the confined Brazilian test. *J. Geophys. Res.* 71 (10), 2651–2659.
- Jansen, D., Carlson, S., Young, R., Hutchins, D., 1993. Ultrasonic imaging and acoustic emission monitoring of thermally induced microcracks in Lac du Bonnet granite. *J. Geophys. Res. Solid Earth* 98 (B12), 22231–22243.
- Jiao, Y.Y., Zhang, X.L., Zhang, H.Q., Li, H.B., Yang, S.Q., Li, J.C., 2015. A coupled thermo-mechanical discontinuum model for simulating rock cracking induced by temperature stresses. *Comput. Geotech.* 67, 142–149.
- Johnson, B., Gangi, A., Handin, J., 1978. Thermal cracking of rock subjected to slow, uniform temperature changes. 19th US Symposium on Rock Mechanics (USRMS).
- Kawamoto, R., Andò, E., Viggiani, G., Andrade, J.E., 2016. Level set discrete element method for three-dimensional computations with triaxial case study. *J. Mech. Phys. Solids* 91, 1–13.
- Kawamoto, R., Andò, E., Viggiani, G., Andrade, J.E., 2018. All you need is shape: predicting shear banding in sand with LS-DEM. *J. Mech. Phys. Solids* 111, 375–392.
- Kim, J., Kwon, S., Sanchez, M., Cho, G., 2011. Geological storage of high level nuclear waste. *KSCE J. Civ. Eng.* 15 (4), 721–737.
- Lee, S.H., Ghassemi, A., 2010. Thermo-poroelastic analysis of injection-induced rock deformation and damage evolution. In: *Proceedings Thirty-Fifth Workshop on Geothermal Reservoir Engineering*.
- Li, D., Wong, L.N.Y., 2013. The Brazilian disc test for rock mechanics applications: review and new insights. *Rock Mech. Rock Eng.* 46 (2), 269–287.
- Li, S., Li, X., Zhang, D., 2016. A fully coupled thermo-hydro-mechanical, three-dimensional model for hydraulic stimulation treatments. *J. Nat. Gas Sci. Eng.* 34, 64–84.
- Ma, G., Wang, X., Ren, F., 2011. Numerical simulation of compressive failure of heterogeneous rock-like materials using SPH method. *Int. J. Rock Mech. Min. Sci.* 48 (3), 353–363.
- Neveu, A., Artoni, R., Richard, P., Descantes, Y., 2016. Fracture of granular materials composed of arbitrary grain shapes: a new cohesive interaction model. *J. Mech. Phys. Solids* 95, 308–319.
- Pandey, S., Chaudhuri, A., Kelkar, S., 2017. A coupled thermo-hydro-mechanical modeling of fracture aperture alteration and reservoir deformation during heat extraction from a geothermal reservoir. *Geothermics* 65, 17–31.
- Potyondy, D., Cundall, P., 2004. A bonded-particle model for rock. *Int. J. Rock Mech. Min. Sci.* 41 (8), 1329–1364.
- Scholtès, L., Donzé, F., 2013. A DEM model for soft and hard rocks: role of grain interlocking on strength. *J. Mech. Phys. Solids* 61 (2), 352–369.
- Scholtès, L., Donzé, F., Khanal, M., 2011. Scale effects on strength of geomaterials, case study: coal. *J. Mech. Phys. Solids* 59 (5), 1131–1146.
- Wang, M., Wang, J., Pan, N., Chen, S., 2007. Mesoscopic predictions of the effective thermal conductivity for microscale random porous media. *Phys. Rev. E* 75 (3), 036702.
- Wang, Z., Jin, X., Wang, X., Sun, L., Wang, M., 2016. Pore-scale geometry effects on gas permeability in shale. *J. Nat. Gas Sci. Eng.* 34, 948–957.
- Wanne, T., Young, R., 2008. Bonded-particle modeling of thermally fractured granite. *Int. J. Rock Mech. Min. Sci.* 45 (5), 789–799.
- Wei, C., Zhu, W., Yu, Q., Xu, T., Jeon, S., 2015. Numerical simulation of excavation damaged zone under coupled thermal-mechanical conditions with varying mechanical parameters. *Int. J. Rock Mech. Min. Sci.* 75, 169–181.
- Xia, M., Zhao, C., Hobbs, B., 2014. Particle simulation of thermally-induced rock damage with consideration of temperature-dependent elastic modulus and strength. *Comput. Geotech.* 55, 461–473.
- Yu, Q., Ranjith, P., Liu, H., Yang, T., Tang, S., Tang, C., Yang, S., 2015. A mesostructure-based damage model for thermal cracking analysis and application in granite at elevated temperatures. *Rock Mech. Rock Eng.* 48 (6), 2263–2282.
- Zhao, Z., 2016. Thermal influence on mechanical properties of granite: a microcracking perspective. *Rock Mech. Rock Eng.* 49 (3), 747–762.